Report Title: Development of Comprehensive Detailed and Reduced Reaction Mechanisms for Syngas and Hydrogen Combustion

Type of Report: Final Technical

Reporting Period:
Start Date 03/01/2006
End Date 02/28/2009

Principal Author: Professor Chih-Jen Sung

Date Report was Issued: May, 2009

DOE Award No.: DE-FG26-06NT42717

Name and Address of Submitting Organizations:

Principal Investigator

Dr. Chih-Jen Sung
415 Glennan Building
Mechanical and Aerospace Engineering Department
Case Western Reserve University
10900 Euclid Avenue
Cleveland, OH 44106
Tel: (216) 368-2942
Fax: (216) 368-6445
Email: cjs15@case.edu

Subcontractors

Dr. Hai Wang
RTH 506
Department of Aerospace and Mechanical Engineering
University of Southern California
Los Angeles, California 90089-1453
Tel: (213) 740-0499
Fax: (213) 740-8071
Email: haiw@usc.edu

Dr. Angela Violi
2150 G.G. Brown
Mechanical, Chemical, and Biomedical Engineering
University of Michigan
2350 Hayward Street
Ann Arbor, MI 48109
Tel: (734) 615-6448
Fax: (734) 647-9379
Email: avioli@umich.edu

DISCLAIMER

ABSTRACT

The collaborative research initiative culminated in amassing a substantial combustion database of experimental results for dry and moist mixtures of syngas and hydrogen (SGH), including autoignition times using a rapid compression machine as well as laminar flame speeds using a counterflow twin-flame configuration. These experimental data provided the basis for assessment of the kinetics of SGH combustion at elevated pressures using global uncertainty analysis methods. A review of the fundamental combustion characteristics of H_2/CO mixtures, with emphasis on ignition and flame propagation at high pressures was also conducted to understand the state of the art in SGH combustion. Investigation of the reaction kinetics of $CO+HO_2\bullet \rightarrow CO_2 + \bullet OH$ and $HO_2+OH \rightarrow H_2O+O_2$ by ab initio calculations and master equation modeling was further carried out in order to look into the discrepancies between the experimental data and the results predicted by the mechanisms.

Table of Contents

1. EXECUTIVE SUMMARY

A collaborative research effort that involves researchers from Case Western Reserve University, University of Southern California, and University of Michigan aims to provide experimental database of high fidelity and develop comprehensive and computationally efficient reaction mechanism for facilitating the design of SGH fuel combustors. Using CO, H_2, H_2O mixtures simulating SGH fuels, fundamental combustion datasets to be obtained experimentally include flame speeds and ignition delay times, with parametric variations of fuel composition, preheat temperature, and pressure. This critical database is needed for validation of chemical kinetics of syngas combustion and is used in conjunction with computation methods, such as global uncertainty analysis, to assess the performance of the literature reaction mechanisms. The present assessment revealed discrepancies in the existing value of a key reaction, $CO+HO_2\bullet \rightarrow CO_2 + \bullet OH$. Reaction kinetics of this reaction was investigated theoretically and a new rate expression was suggested which corrected the noted disagreement in predictions of the existing mechanisms for syngas combustion.

The present study is broken down into the following major projects:

i. Extensive experimental data for autoignition of dry syngas mixtures at elevated pressures in a rapid compression machine were obtained. Experiments were done for pressures 15–50 bar and temperatures from 950 to 1100 K. Ignition delays were measured for stoichiometric compositions of $CO + H_2$ containing between 0 and 80% CO in the total fuel mixture. Contrary to the simulated results, the experimental data showed an unequivocal monotonic increase in ignition delay as the proportion of CO in the mixture was raised.

ii. Assessment of the kinetics of syngas combustion at elevated pressures using global uncertainty analysis methods was conducted to trace the reason behind the discrepancy of the experimental data and computed results.

iii. Extensive experimental data of flame propagation for moist syngas mixtures at elevated unburned temperature of 323 K, with water additions of 0–35% in syngas mixture, H_2/CO molar ratios of 5/95 – 100/0, and equivalence ratios of 0.3–0.9, were obtained. In this study, for the CO-rich mixtures (small H_2/CO ratio) investigated, it was found that laminar flame speed varies non-monotonically with addition of water – first increases with increasing amount of water addition, reaches a maximum value, and then decreases. A detailed integrated flux flow analysis was further conducted to understand the controlling chemistry responsible for such a non-monotonic flame response.

iv. A review of the fundamental combustion characteristics of H_2/CO mixtures, with emphasis on ignition and flame propagation at high pressures was done to understand the state of the art.

v. Experimental data for autoignition of moist syngas mixtures at elevated pressures using a rapid compression machine were obtained. This work investigated the effect of water addition on ignition delays of stoichiometric syngas mixtures with varying H_2/CO molar ratios. While the compressed charge pressure was fixed at P_C=30 bar, RCM experiments were conducted for mixtures with H_2/CO molar ratios of 100/0, 50/50, and 5/95, over a compressed temperature range of T_C=930–1080 K. For given H_2/CO molar ratio and compressed conditions, the effect of water addition on ignition delay was studied for molar percentages of water in the reactive mixture of 0%, 2.5%, 5%, and 10%. For the

conditions investigated, the presence of 5% and 10% water vapor was shown to promote autoignition, even for the pure hydrogen cases.

vi. Investigation of the reaction kinetics of $CO+HO_2\bullet \rightarrow CO_2 + \bullet OH$ by ab initio calculations and master equation modeling was conducted.

vii. Investigation of the reaction kinetics of $HO_2+OH \rightarrow H_2O+O_2$ by ab initio calculations and master equation modeling was carried out.

2. REPORT DETAILS

2.1. Autoignition of Moist Syngas Mixtures at Elevated Pressures

2.1.1. Experimental Method

The experimental setup consists of a rapid compression machine (RCM), a flow control/supply system, and a mixing chamber. Both the RCM and the mixing chamber along with the manifolds have a provision for heating up to a maximum temperature of 400 K. For the current study, in order to cover the entire range of water addition, the whole experimental setup is heated to a temperature of 350 K. This RCM consists of a reaction chamber in which the reactant gases are compressed by a creviced piston arrangement. The creviced piston is driven by an arrangement of the pneumatic piston and high-pressure air tank. It is held in place by an arrangement of the hydraulic cylinder. A trigger of a solenoid valve releases the pressure of the hydraulic chamber, and thus the piston arrangement moves forward by the pneumatic system. Towards the end of the compression stroke, the piston is decelerated and finally stopped by the piston stopping groove. The compression stroke of the RCM takes an average time of 30 ms. The end reaction chamber is equipped with a pressure transducer and a thermocouple. It is also provided with quartz windows for any required optical access. Figure 1 shows the schematic of the RCM with general details of the end reaction chamber and the creviced piston. The compression ratio of the machine can be changed by changing the clearance and/or the stroke length. Split shims are used to vary the clearance between hydraulic cylinder and the reaction chamber and the stroke can be adjusted by using spacers.

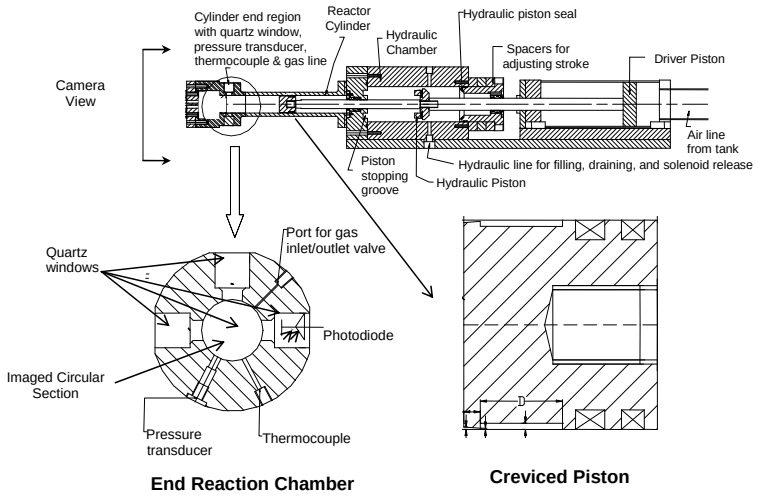

Figure 1: Schematic of the present rapid compression machine, the end reaction chamber, and the creviced piston head.

The mixing chamber consists of an airtight stainless steel tank, with an arrangement of magnetic stirrer for proper mixing of the constituents. The tank is provided with a rupture disc as a safety measure against accidental overpressure within the mixing tank. The gas mixtures are prepared at room temperature, gases are filled into the mixing chamber by the method of partial pressures, while water is gravimetrically measured and injected into the chamber. High-purity gases are used for this study: CO (99.998%), H_2 (99.999%), N_2 (99.999 %), O_2 (99.993 %), and Ar (99.999%). Moreover, deionized water (TDS<0.03571 ppm and ρ>14 MΩ-cm) is used.

Mix No.	R_{CO}	Mole Percentage of Constituents (%)						
		H_2	CO	O_2	CO_2	H_2O	N_2	Ar
1	0.00	12.500	0.000	6.250	0.000	0.000	18.125	63.125
2	0.95	0.625	11.875	6.250	0.000	0.000	16.590	64.660
3	0.50	6.250	6.250	6.250	0.000	0.000	17.315	63.935
4	0.00	12.500	0.000	6.250	0.000	2.500	13.988	64.762
5	0.95	0.625	11.875	6.250	0.000	2.500	12.455	66.295
6	0.50	6.250	6.250	6.250	0.000	2.500	13.182	65.568
7	0.00	12.500	0.000	6.250	0.000	5.000	9.850	66.400
8	0.95	0.625	11.875	6.250	0.000	5.000	8.320	67.930
9	0.50	6.250	6.250	6.250	0.000	5.000	9.048	67.202
10	0.00	12.500	0.000	6.250	0.000	10.000	1.580	69.670
11	0.95	0.625	11.875	6.250	0.000	10.000	0.000	71.250
12	0.50	6.250	6.250	6.250	0.000	10.000	0.780	70.470

Table 1: Test matrix for ignition delay experiments.

Experiments to be presented here are conducted at stoichiometric condition (ϕ=1.0) for three different CO/H_2 ratios of R_{CO}=0, 0.5, and 0.95 with molar percentage of water in the mixture of 0%, 2.5%, 5%, and 10%, where R_{CO} is defined as the molar fraction of CO in the combined H_2+CO fuel mixture. Nitrogen and argon are used to adjust the specific heats of the gas mixtures to approximately the same value over the temperature range of 350–1000 K. Table 1 lists the mixture compositions conducted in the RCM experiments.

For a given mixture composition, the compressed gas temperature at the end of compression, T_C, is varied by altering the compression ratio, whereas the desired pressure at the end of compression, P_C, is obtained by varying the initial pressure of the reactive mixture. The compressed gas temperature is determined by the adiabatic core hypothesis.

2.1.2. Results and Discussion

Figure 2 shows the effect of water addition on ignition delay over a range of compressed temperatures for the pure hydrogen case (R_{CO}=0). The initial mixture temperature is T_0=350 K. It is seen that ignition delay increases with 2.5% water addition, as compared to the dry condition. However, the ignition delay decreases as water addition is increased to 5%, indicating higher reactivity of the moist mixture. The ignition delay further decreases with 10% water addition, as demonstrated in Fig. 2.

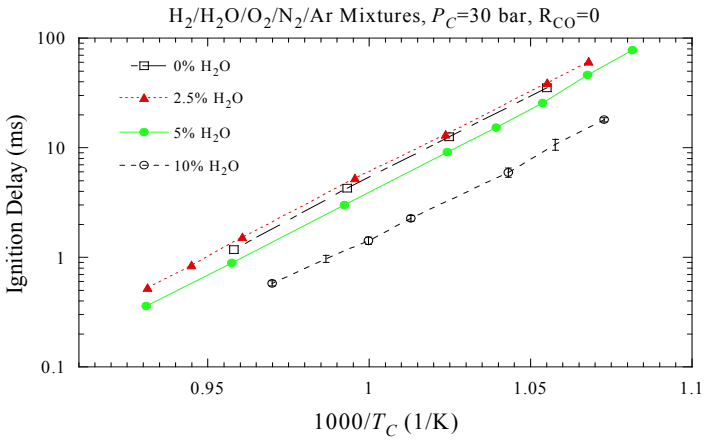

Figure 2: Ignition delays at 30 bar for ϕ=1, T_0=350 K, and R_{CO}=0 with water addition (0–10%).

Figures 3 and 4 show the ignition delay results for R_{CO}=0.95 and 0.5, respectively. It is also seen that with 5% and 10% water addition, ignition delay is reduced as compared to the corresponding dry case. At 2.5% water addition, however, the ignition response depends on the compressed charge temperature. In the case of R_{CO}=0.95, while at higher compressed temperatures (T_C>1030 K) the ignition delay is higher when compared to 0% water addition, the ignition delay becomes shorter when T_C<1030 K. For R_{CO}=0.5, with 2.5% water addition, the ignition delay is slightly more than the case without water addition for higher compressed temperatures, but at T_C<1010 K, the ignition delay is faster when compared to the dry case.

The ignition delay data at P_C=30 bar and T_C~1010 K are further plotted as a function of R_{CO} in Fig. 5 for comparison. It is seen that at lower values of R_{CO}, the ignition delay is slower at 2.5% water addition, with comparison to the dry case. At R_{CO}=0.5 the difference is minimum, and at R_{CO}=0.95, the ignition delay becomes faster. It is also noted that with 5% and 10% water addition, the ignition delays are faster for all values of R_{CO}. However, the extent of reduction is minimum for R_{CO}=0, increases at R_{CO}=0.5, and is largest at R_{CO}=0.95.

The above experimental results indicate a complex behavior of ignition delay with water addition, which needs further study to understand fully. Constant volume, adiabatic calculations are conducted using SENKIN for pure hydrogen mixtures (R_{CO}=0) at initial conditions of 30 atm and 1000 K to examine and compare the trends predicted by different reaction mechanisms reported in the literature.

Because of different ignition delay values predicted by different mechanisms, for a fair comparison regarding the ignition delay response with respect to water addition, the predicted ignition delays in the water addition range of 0–10% are normalized by the ignition delay with 0% H_2O addition. The normalized ignition delays, [$\tau(x\%\ H_2O)/\tau(0\%\ H_2O)$], obtained by using various mechanisms, are plotted and compared as a function of percentage water addition in Fig. 6. It can be seen that the effect of water addition on ignition delay observed in our RCM experiments is only captured by the mechanism of O'Conaire *et al*. 0 for pure hydrogen. The other reported H_2/CO mechanisms tested fail to capture the experimental trend. Further experiments at other pressures are required to fully understand the ignition response with water addition. Flux flow analysis using the mechanism of O'Conaire *et al.* 0 will also be helpful to understand the chemical kinetic aspect for the effect of water addition on ignition delay.

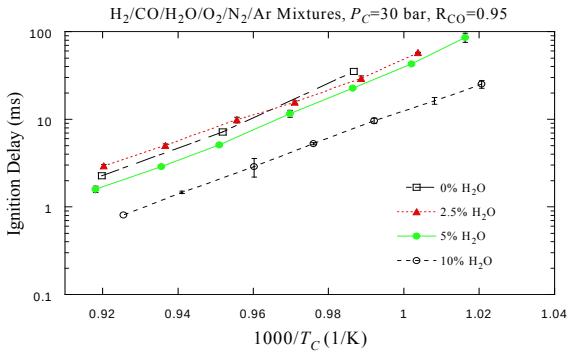

Figure 3: Ignition delays at 30 bar for ϕ=1, T_0=350 K, and R_{CO}=0.95 with water addition (0–10%).

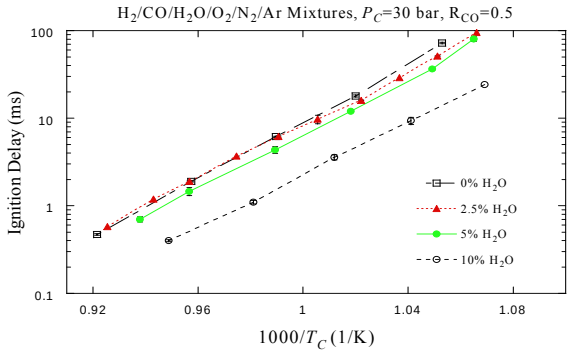

Figure 4: Ignition delays at 30 bar for ϕ=1, T_0=350 K, and R_{CO}=0.5 with water addition (0–10%).

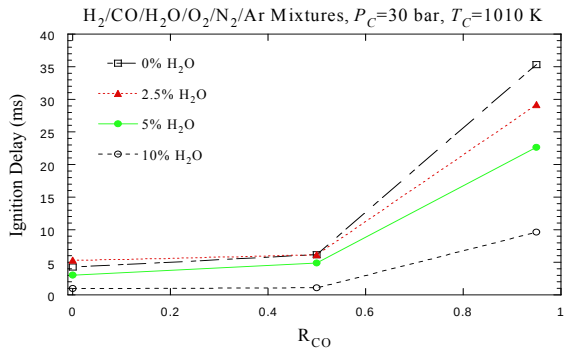

Figure 5: Comparison of ignition delays at P_C=30 bar and T_C~1010 K for ϕ=1, T_0=350 K, and various R_{CO} with water addition (0–10%).

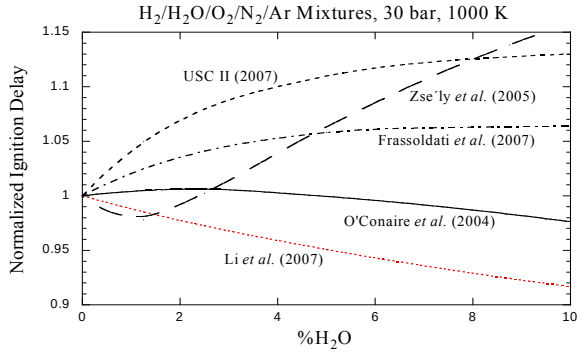

Figure 6: Comparison of predicted ignition delay trends due to water addition for different literature mechanisms.

2.1.3. Conclusions

- Ignition delay experiments over a wide range of H_2/CO ratios were conducted using an RCM, with special emphasis on the effect of water addition on autoignition.
- The study so far reveals a complex dependence of ignition delay with water addition for various values of R_{CO}.
- For the pure hydrogen case (R_{CO}=0), it is seen that with 2.5% water addition, the ignition delay increases, and further water addition leads to a decrease in the ignition delay time.
- For the CO rich case (R_{CO}=0.95), the temperature dependence of ignition delay at 2.5% water addition is observed. While at higher temperatures the ignition delay with 2.5% water addition is higher than the dry case, at lower temperatures the ignition delay with 2.5% water addition becomes lower.
- For R_{CO}=0.95, with further water addition at 5% and 10%, the ignition delays consistently decrease as compared to the dry case, for the conditions tested.
- Further experiments at other pressures are required to fully understand the ignition response with water addition.
- Flux flow analysis using the Lawrence Livermore mechanism for pure hydrogen can be helpful to understand the chemical kinetic aspect for the effect of water addition on ignition delay time.

2.2. Laminar Flame Speeds of Moist Syngas Mixtures

Using the counterflow twin-flame configuration, this work experimentally investigates the effect of the presence of water vapor on the laminar flame speeds of syngas mixtures with various composition and equivalence ratios on the lean side. Experimental results presented here are for the mixtures with H_2/CO molar ratios varying from 5/95 to 100/0 at preheat temperature of 323 K and under atmospheric pressure. For a given equivalence ratio, the variation of the measured laminar flame speed with varying amount of water addition is demonstrated. The experimental laminar flame speeds are then compared to the computed values using chemical kinetic mechanisms reported in the literature.

2.2.1. Experimental Method

Figure 7 shows a schematic of the experimental setup. The setup consists of flow control and mixing system, counterflow burner apparatus, and a digital particle image velocimetry system. The flow control system consists of calibrated choked orifices which are used to meter the flow of desired amount of gases. The water is injected into the system by a positive displacement syringe pump. A part of the N_2 flow is diverted and heated for atomization of water. For complete vaporization, the atomized water with the heated N_2 is passed through a heated vaporization chamber. The rest of nitrogen as well as a part of oxygen and carbon-monoxide are passed through nebulizers. All gases are then mixed in the mixing section before being divided and discharged through two opposing convergent nozzle burners. The entire burner assembly is electrically heated to obtain the desired unburned gas temperature at the nozzle exit. The exit nozzle diameter is 13 mm, while the separation distance between two opposing nozzle is 12 mm.

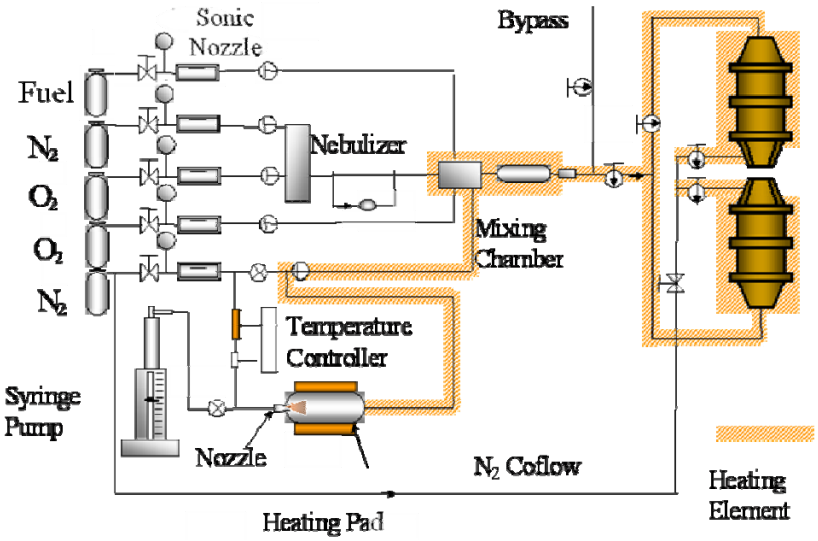

Figure 7: Schematic of the flow control and mixing system along with the counterflow burner assembly.

The resulting counterflow twin flames are shielded from the ambience by a nitrogen co-flow. In this study, the high-purity gases are used: CO (99.5%), H_2 (99.995%), N_2 (99.98 %), andO_2 (99.98 %).

2.2.2. Results and Discussion

Laminar flame speed measurements are conducted for H_2/CO molar ratios varying from $\eta_{H2/CO}$=0.053 (i.e. H_2/CO=5/95) to $\eta_{H2/CO}\rightarrow\infty$ (i.e. H_2/CO: 100/0) and for percentages of water

content of ξ_{H2O}=0–35%. Here, ξ_{H2O} is defined as $[(X_{H2O})/(X_{H2}+X_{CO}+X_{H2O})]\times 100\%$ in the fuel mixture, where X_i is the mole fraction of species i. The results are studied and discussed under three different cases – $\eta_{H2/CO}$=0.053, $\eta_{H2/CO}\rightarrow\infty$, and $\eta_{H2/CO}$=1.

For $\eta_{H2/CO}$=0.053, Fig. 8 shows the experimentally determined laminar flame speed data for equivalence ratios of ϕ=0.6 and 0.7. Computed laminar flame speeds using the mechanism of Li *et al.* [2] are also plotted for comparison. It is seen that the effect of water addition on laminar flame speed exhibits a non-monotonic behavior. Specifically, the laminar flame speed increases with addition of water initially from ξ_{H2O}=0% to around ξ_{H2O}=15% and then decreased from around ξ_{H2O}=15% to ξ_{H2O}=35%. Similar trends are also observed for ϕ=0.8 and 0.9, as shown in Fig. 9. The computed flame speed response using the mechanism of Li *et al.* [2] also demonstrates a similar non-monotonic trend. In general, the experimental data and the computed laminar flame speeds agree fairly well.

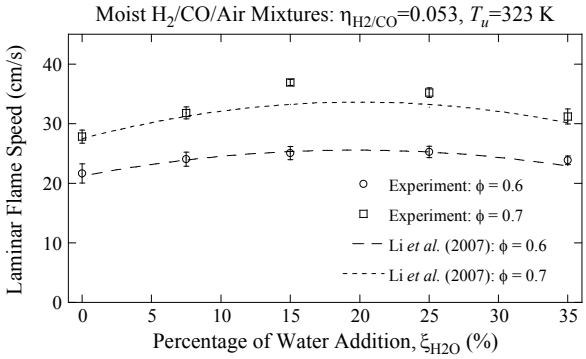

Figure 8: Variation of laminar flame speeds with water addition. ϕ=0.6 and 0.7, $\eta_{H2/CO}$=0.053, T_u=323 K. Computed results using the mechanism of Li *et al.* [2] are also included.

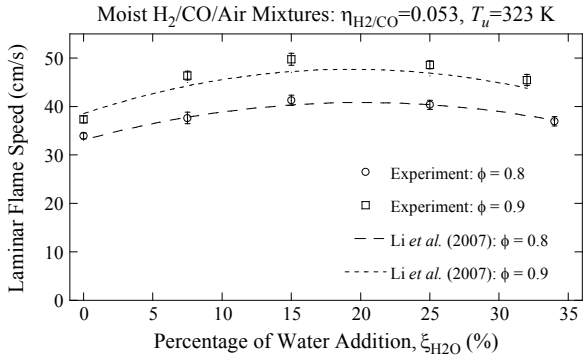

Figure 9: Variation of laminar flame speeds with water addition. ϕ=0.8 and 0.9, $\eta_{H2/CO}$=0.053, T_u=323 K. Computed results use the mechanism of Li *et al.*[2].

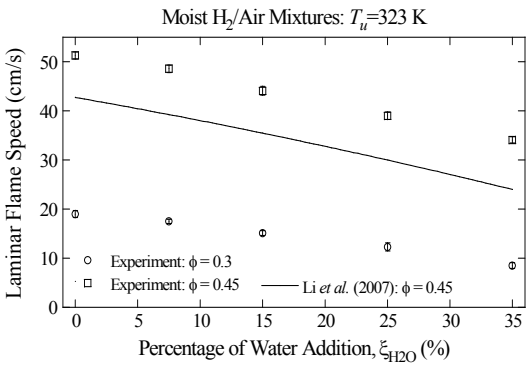

Figure 10: Variation of laminar flame speeds with water addition. ϕ=0.3 and 0.45, $\eta_{H2/CO}\rightarrow\infty$, T_u=323 K. Computed results using the mechanism of Li *et al.* [2] are also included.

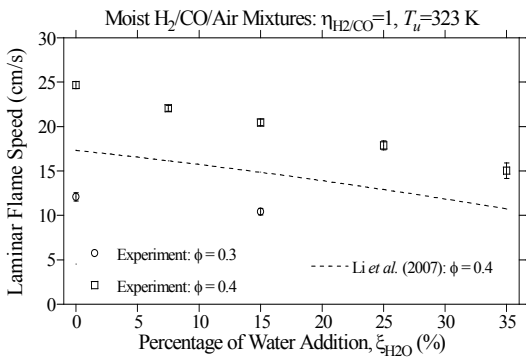

Figure 11: Variation of laminar flame speeds with water addition. ϕ=0.3 and 0.4, $\eta_{H2/CO}$=1, T_u=323 K. Computed results use the mechanism of Li *et al.* [2].

For $\eta_{H2/CO}\rightarrow\infty$, Fig. 10 shows the experimentally determined laminar flame speed data for equivalence ratios of ϕ=0.3 and 0.45. Computed laminar flame speeds using the mechanism of Li *et al.* [2]are also plotted for comparison. It is seen that the effect of water addition on laminar flame speed for this case exhibits a strictly monotonically decreasing trend throughout the range of water addition. The computed flame speed response using the mechanism of Li *et al.* [2] also

demonstrates a similar trend. However, this mechanism largely under-predicts the flame speed values for the high H_2 content lean mixtures.

For $\eta_{H2/CO}$=1.000, Fig. 11 shows the experimentally determined laminar flame speed data for equivalence ratios of ϕ=0.3 and 0.4. Computed laminar flame speeds using the mechanism of Li *et al*. [2] are also plotted for comparison. It is seen that the effect of water addition on laminar flame speed for this case also exhibits a strictly monotonically decreasing trend throughout the range of water addition. Similar trends are observed for ϕ=0.5 and 0.6, as shown in Fig. 12. The computed flame speed response using the mechanism of Li *et al.* [2] also demonstrates a similar trend. For this case, although the mechanism under-predicts the flame speed values for this fuel mixture, it is to a lesser extent when compared with predicted values for the case of $\eta_{H2/CO}\rightarrow\infty$.

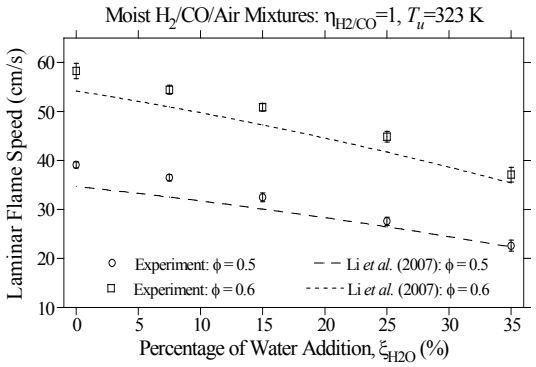

Figure 12: Variation of laminar flame speeds with water addition. ϕ=0.5 and 0.6, $\eta_{H2/CO}$=1, T_u=323 K. Computed results using the mechanism of Li *et al.*[2]are also included.

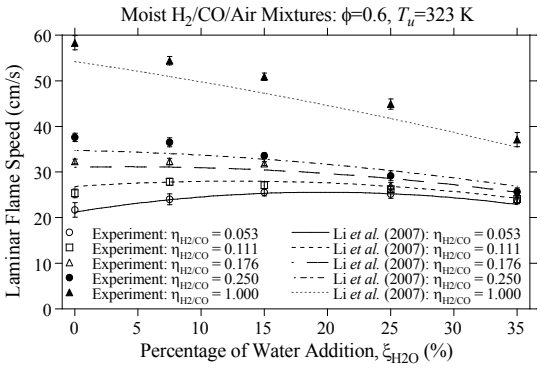

Figure 13: Variation of laminar flame speed with water addition for ϕ=0.6, T_u=323 K, and $\eta_{H2/CO}$=0.053, 0.111, 0.176, 0.25, and 1.

To see the effect of water addition for different H_2/CO ratios, flame speed measurements are carried out at H_2/CO ratios of $\eta_{H2/CO}$=0.053 (i.e. H_2/CO=5/95), $\eta_{H2/CO}$=0.111 (i.e. H_2/CO=10/90), $\eta_{H2/CO}$=0.176 (i.e. H_2/CO=15/85), $\eta_{H2/CO}$=0.25 (i.e. H_2/CO=20/80) and $\eta_{H2/CO}$=1 (i.e. H_2/CO=50/50). Water content of the fuel mixture is in the range of ξ_{H2O}=0–35%. Figure 13 summarizes the data, and shows the comparison of experimental and computed laminar flame speeds. It is seen from Fig. 13 that the computed laminar flame speeds agree reasonably well with the experimental data, for the conditions investigated. The non-monotonic trend of laminar flame speed with water addition and the diminution in the non-monotonic trend with increase in H_2/CO ratio is also captured in simulations.

Chemical kinetic analysis further illustrates that for lower values of H_2/CO ratio, the positive chemical effect of water addition is much more pronounced than the negative thermal effect for lower percentages of water addition. However, as the percentage of water addition in the fuel mixture is increased beyond a critical value, the negative thermal effect becomes dominant, leading to the reduction in laminar flame speed. For higher values of H_2/CO ratio, it is seen that the flame speed response is monotonically decreasing with water addition, indicating the dominance of the thermal effect of water addition throughout the range. Chemical kinetic analysis also shows that under these conditions the chemical effect of water addition is not pronounced.

2.2.3. Conclusions

- For the CO-rich cases (lower values of H_2/CO molar ratio), the variation of laminar flame speed with water addition is non-monotonic.
- Detailed flux flow analysis was conducted to identify the controlling chemistry accounting for this non-monotonic behavior.
- Such a non-monotonic flame speed response with water addition diminishes as the H_2/CO ratio is increased.
- There exists a critical value of water addition at which laminar flame speed peaks and starts decreasing thereafter. This critical value of water addition decreases with increasing H_2/CO ratio.
- Beyond a critical value of H_2/CO ratio (i.e. H_2-rich cases), laminar flame speed decreases monotonically with increasing water addition.
- While there is a reasonably good agreement between the computed and experimental laminar flame speed data for lower values of H_2/CO ratio, the existing reaction mechanisms under-predict laminar flame speeds for the cases with higher H_2/CO ratios. The discrepancy increases further with leaner equivalence ratios.
- The laminar flame speed data thus obtained can be used to improve and optimize the chemical kinetics mechanism for the oxidation of H_2/CO.

2.3. Reaction Kinetics of $CO+HO_2 \rightarrow$ Products

2.3.1. Results and Discussion

An experimental and numerical study, using uncertainty analysis of the most important parameters, is conducted to evaluate the mechanisms for the combustion of $CO+H_2$ mixtures at high pressures in the range 15–50 bar and temperatures from 950 to 1100 K. Experiments are performed in a rapid compression machine. Autoignition delays were measured for stoichiometric compositions of $CO+H_2$, with varying proportion of $R_{CO}=[CO]/([CO]+[H_2])$, while keeping the combined $[CO]+[H_2]$ constant, where brackets indicate molar concentrations of respective species. The experimental results show an unequivocal monotonic increase in ignition delay as the proportion of CO in the mixture is raised, whereas simulations using the reaction mechanisms [2] show a qualitatively different behaviour of almost no sensitivity to R_{CO} till it reaches 0.8, as shown in Fig. 14.

Global uncertainty analyses, including Morris and Monte Carlo Analyses, are then applied to the kinetic model of Davis *et al.* [3] in order to trace the origins of this discrepancy. The analyses take into account the uncertainties in all rate parameters in the model, which is a pre-requisite for evaluation against ignition delay data. Morris analyses identify the reaction, $CO+HO_2\bullet \rightarrow CO_2 + \bullet OH$, as the most important reaction which leads to largest absolute mean perturbation and standard deviation in predicted ignition delay when rate parameters for all other reactions are varied within their uncertainty range. Figure 15 shows a scatter plot from Monte Carlo analysis which reflects the values for ignition delay that are predicted within the ranges of uncertainties of all other pre-exponential factors when log A of the reaction, $CO+HO_2\bullet \rightarrow CO_2 + \bullet OH$, takes set values over the range $-12 < \log A < -10$. With commonly used value of log A, experimentally observed ignition delay is predicted in very few cases. This suggests that the accepted value of log A is incorrect. $\log A < -11$ would fix it but the present analysis based on ignition delay

measurements does not permit us to do more than indicate that the overall reaction rate is too fast. This constraint arises from the uncertainty in other rate parameters that gives the scatter in the predicted ignition delays – which is problem for any model validation using ignition delay data. Corrected parameters cannot be generated for this reaction solely from ignition delay evaluations. Direct experimental or theoretical approaches are therefore required to determine the rate parameters.

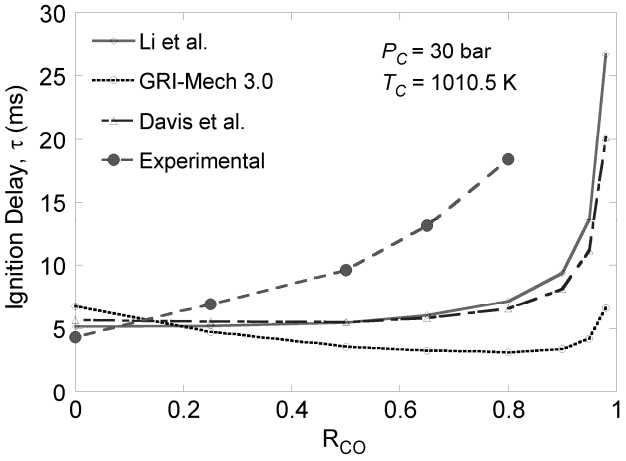

Figure 14: Comparison of experimental and computed results, showing the effect of CO addition on ignition delay. Molar composition: $(H_2+CO)/O_2/N_2/Ar$ = 12.5/6.25/18.125/63.125. Conditions at TDC: P_C=30 bar and T_C=1010.5 K.

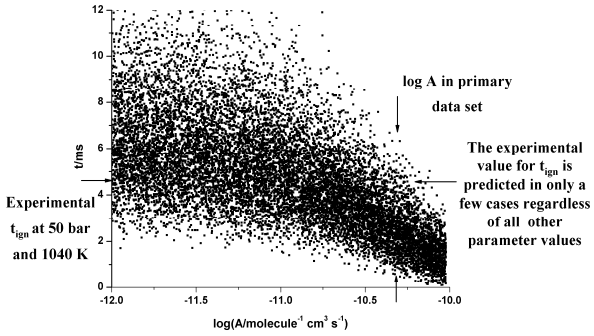

Figure 15: Monte Carlo analysis from 13000 simulations for variation of the pre-exponential factor for $CO+HO_2\bullet \rightarrow CO_2 + \bullet OH$ over the range -12 < log A < -10. Pre-exponential terms for the remaining reactions in the scheme are varied within the estimated uncertainty. In the primary data set log (A / cm^3 molecule^{-1} s^{-1}) = -10.3, as marked (vertical arrows). The experimentally measured ignition delay is 4.6 ms (horizontal arrows).

The reaction kinetics of $CO+HO_2\bullet \rightarrow CO_2 + \bullet OH$ is subsequently studied using the single-reference CCSD(T) method with Dunning's cc-PVTZ and cc-PVQZ basis sets and multireference CASPT2 methods. It is found that the classical energy barriers are about 18 and 19 kcal/mol for $CO+HO_2\bullet$ addition following the *trans* and *cis* paths, as shown in Fig. 16. Figure 16 also demonstrates that the HOOC•H adduct has a well defined local energy minimum in the *trans* configuration, but the *cis*-conformer is either a very shallow minimum or an inflection point on the potential energy surface.

This observation leads us to treat the *cis*-pathway by the classical transition state theory and the *trans*-pathway by a Master Equation analysis. The computation showed that the overall rate is independent of pressure up to 500 atm. Upon a careful treatment of the hindered internal rotations in the HOOC•H adduct and relevant transition states, the rate coefficient expression for this reaction is obtained as k (cm^3/mol.s) = $1.6 \times 10^5\ T^{2.18}\ e^{-9030/T}$ for $300 \leq T \leq 2500$ K. Lastly, we examine the accuracy of the previously proposed Davis *et al.* [3] model by updating only three rate coefficients: k_1 based on the current study, the rate coefficient of $CO + \bullet OH \rightarrow CO_2 + H\bullet$ from Joshi and Wang [5], and rate coefficient for $HO_2\bullet + OH \rightarrow H_2O + O_2$ evaluated in Sivaramakrishnan *et al.* [6]. Figure 17 shows the comparison of experimental and computed ignition delays for RCM experiments at 30 bar, before and after these updates. It is seen that the updates just discussed led to drastic improvement of the predictions, as expected. The

improvement was brought almost entirely from the revision of the rate coefficient of $CO+HO_2\bullet \rightarrow CO_2 + \bullet OH$.

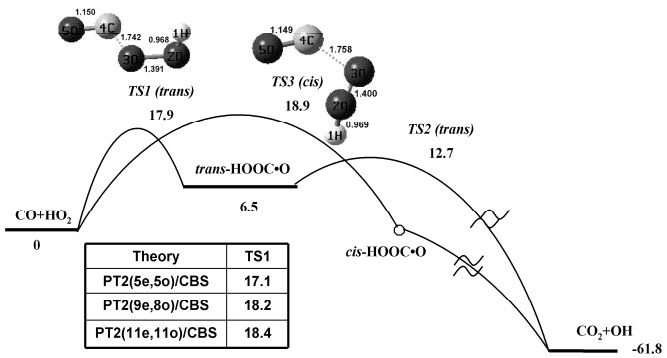

Figure 16: Potential energy diagram for $CO + HO_2\bullet \rightarrow CO_2 + \bullet OH$. The energy values are determined using the CCSD(T)/CBS method, and include zero-point energy corrections.

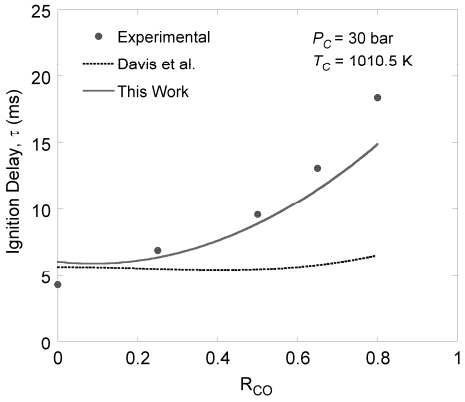

Figure 17: Prediction of RCM ignition delay times at P_C = 30 bar and T_C around 1010.5 K. Molar composition: $(H_2+CO)/O_2/N_2/Ar$ = 12.5/6.25/18.125/63.125. Solid lines: updated model from this work; dashed line: model of Davis *et al.* [3].

2.3.2. Conclusions

- Significant discrepancies exist in the literature chemical kinetic models of syngas combustion.
- Global uncertainty analysis identify the reaction $CO+HO_2\bullet \rightarrow CO_2 + \bullet OH$ as the most important reaction causing the discrepancy between the predicted and the experimental values of the ignition delay times.
- Theoretical calculations for the key reaction, $CO+HO_2\bullet \rightarrow CO_2 + \bullet OH$, resolved some discrepancies of the existing mechanisms at elevated pressures.

2.4. Reaction Kinetics of $HO_2 + OH \rightarrow H_2O + O_2$

2.4.1. Results and Discussion

In current models of H_2/CO combustion, a key uncertainty stems from the rate constant of $HO_2+OH \rightarrow H_2O+O_2$ [R1]. Early observations show that the rate coefficient k_1 scatters in the range $(2\sim6)\times10^{13}$ cm^3/mol-s at the room temperature. Several studies suggested that k_1 has a negative activation energy. For example, Sridharan *et al.* [13] reported that at a pressure of 2.5 Torr k_1 (cm3/mol-s) = 10^{13} exp (416/T) for 252≤ T ≤ 420 K. Keyser [16] reported that k_1 (cm^3/mol-s) = 1.1×10^{13} exp (250/T) at 1 Torr over the temperature range from 254 to 382 K.

Troe, Hippler and coworkers suggested that from 970 to 1220 K k_1 reaches a minimum at ~1000 K, and it increases rapidly towards higher temperatures. Their measurements were made by following the kinetics of H_2O_2 thermal decomposition behind reflected shock waves, in which R1 was only a secondary reaction. In a recent high-pressure shock tube H_2/CO oxidation study [22], R1 was identified as critical to model the CO oxidation rates over the pressure range of 25 to 450 atm and the temperature from 1000 to 1500 K.

The peculiar temperature dependence reported by Troe and coworkers was found to provide a better agreement between model and experiment. Unfortunately, no experimental data are

available in the intermediate temperature range 420~950 K to confirm the peculiar behavior in k_1. Contrary to the findings of Troe and coworkers, Srinivasan *et al.* [23] found little to no temperature dependency in k_1 from 1237 to 1554 K. In their experiments, they followed the disappearance of •OH in C_2H_5I/NO_2 mixtures behind reflected shock waves, employing a multipass optical system which detects the •OH absorption. The time-dependent decay profile was fitted with a 23-step mechanism by varying the rate constants of •OH + NO_2 ↔ HO_2• + NO and R1. They recommended $k_1 = 3\times10^{13}$ cm3/mol-s as a compromise of 4×10^{13} cm^3/mol-s over the temperature range of 1237 to 1554 K and the previous data [19][21] [24] in the range of (1-6)$\times10^{13}$ cm^3/mol-s for $1200 \le T \le 1700$ K.

In the present work, the temperature and possible pressure dependence of the rate coefficient for R1 is examined by *ab initio* electronic structure calculations. Both singlet and triplet potential energy surfaces are investigated at the CBS-QBH level of theory.

Reaction R1 can occur on both triplet and singlet surfaces. The CBS-QBH potential energy diagrams on the two surfaces are provided in Figs. 18 and 19, separately. The BHandHLYP/6-311++G(d,p) geometry parameters are presented in Fig. 20. On the triplet surface, the reaction follows an H-abstraction pathway. A hydrogen-bonded complex HO...HOO is formed from the barrierless recombination of the reactants •OH and HO2•. Its energy lies 5 kcal/mol below the potential energy of the entrance channel. For the complex to dissociate into the products H_2O and the ground state $^3O_2$, it requires only 1 kcal/mol of energy barrier.

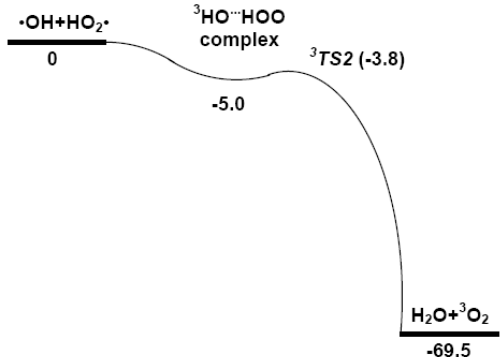

Figure 18: CBS-QBH potential energy diagram for OH• + HO_2• → products on the triplet surface (units: kcal/mol).

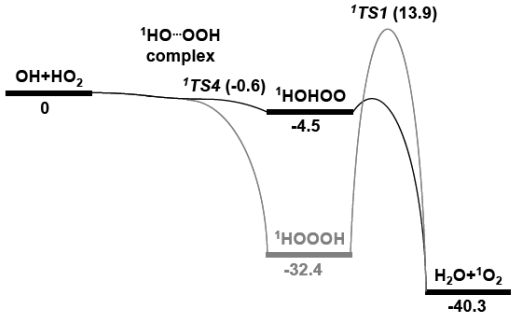

Figure 19: CBS-QBH potential energy diagram for OH• + HO_2• → products on the singlet surface (units: kcal/mol). Grey lines: closed-shell singlet surface; Black lines: open-shell singlet surface.

To be noted, the open-shell singlet ^{1}HOHOO, similar to the triplet complex ^{3}HO...HOO in structure, is only 1 kcal/mol higher in energy. Unfortunately, no results from other methods are available to provide theoretical confirmation for the above results because the geometry optimization fails routinely with these methods. Compared to a previous study [25] for the triplet surface at the MP4/6-31G**//MP2/6- 31G** level of theory, the complex and the critical geometry obtained here are similar in structure, but the critical energy they computed for $^3TS_2$ is as much as 6 kcal/mol higher than the present result. In fact, the complex and critical geometry reported are not a true local minimum and a saddle point, respectively, as one of the out-of-plane torsional frequencies for both structures are imaginary. In the present work, $^3TS_2$ is calculated to have only one imaginary frequency, as expected for a true critical geometry.

Meanwhile, the triplet PES is explored also at several levels of the MP*n* theory. While MP2 and MP4(STQ) fail to provide the transition state, and B3LYP and MP4(SDTQ) fail for both the

complex and transition state, at the MP3 and MP4(DQ) level of theory stationary points are successfully computed; and this is accomplished only when a tight convergence criteria are used. Although similar results can be seen with all methods when applied to the triplet hydrogen-bonded complex HO...HOO, the results for the energy barrier ^{3}TS2 are quite different, as seen in Table 2. The MP*n* methods produce $^3TS_2$ with energies from 6.4 to 6.9 kcal/mol above the entrance channel. In comparison, a procedure similar to CBS/QBH but with geometry optimization at MP4(DQ)/6-311++G(d,p) level of theory (CBS-QMP4DQ) gives a quite low value for ^{3}TS2, about 7.5 kcal/mol below the entrance channel. The CBS-QBH energy is consistent with the results from BHandHLYP/6-6-311++G(d,p) and CBS-QMP4DQ and is probably more reliable than other methods employed here. The reaction enthalpies and energy barriers are presented in Table 2, where the literature values for the enthalpy of reaction are based on the heats of formation given in Table 3. As seen, the CBS-QB3, CBSQBH, and CBS-AMP4DQ methods yield reaction enthalpies within 0.5 kcal/mol of the literature values.

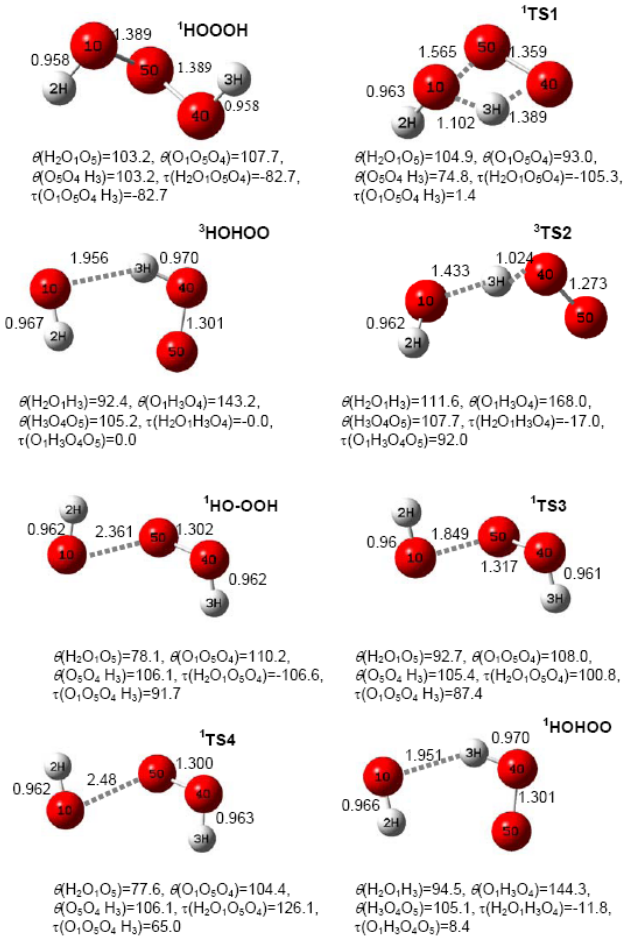

Figure 20: Geometry parameters determined at BHandHL YP/6-311++G(d,p) level of theory. The bond lengths are in Å, and the angles are in degrees.

Table 2: Energies (kcal/mol) at 0 K relative to OH• + HO_2•.

	$H_2O+{}^1O_2$	^{1}HOOOH	^{1}HO-OOH	TS1	TS3	TS4	$H_2O+{}^3O_2$	^{3}HOHO$_2$	^{1}HOHO$_2$	TS2
Literature value							-69.5			
B3LYP/6-31g(d)	-25.9	-30		14.7			-65.2			
BHandHLYP/6-311++g(d,p)	-39.2	-14.0	-1.2	39.2	1.4	-1.4	-61.6	-4.9	-4.9	-2.0
MP2/6-311++g(d,p)	-50.8	-32.6		15			-81.1	-4.7		
MP3/6-311++g(d,p)	-32.8	-21.9		34			-67.5	-4.3		6.4
MP4(DQ)/6-311++g(d,p)	-35.7	-22.1		33.9			-68.8	-4.2	-4.1	6.9
MP4(SDQ)/6-311++g(d,p)	-36.9	-22.9		28.1			-69.6	-4.3		
MP4(SDTQ)/6-311++g(d,p)	-44.1	-28.9					-73.7			
CCSD(T)/cc-pVTZ	-38.3						-68			
G3B3	-40.2	-31.3		16.2			-69.1			
CBS-QBH	-40.3	-32.4		13.9			-69.5	-5.0	-4.0	-3.8
CBS-QMP4DQ	-41.5	-33.2		13.1			-70.0	-4.8	-3.9	-7.5
CBS-QB3	-41.2	-33.4	-0.6	11.7	-6.1	-0.6	-69.8			
CCSD(T)/CBS							-69.4			

Table 3: Literature values of enthalpy of formation (kcal/mol).

Species	$\Delta_f H_{298}$	$\Delta_f H_0$	Reference
•OH	8.9 ±0.07	8.8	(Ruscic et al. 2002)
HO_2•	2.9±0.1	3.6	(Ruscic et al. 2006)[a]
H_2O	-57.8	-57.1	(Chase 1998)

[a] $\Delta_f H_0$ values are obtained from $\Delta_f H_{298}$ and the sensible enthalpy values taken from Chase (1998).

3. LIST OF FIGURES

4. LIST OF TABLES

5. REFERENCES

[1] O'Conaire, M., Curran, H. J., Simmie, J. M., Pitz, W. J. and Westbrook, C. K., *International Journal of Chemical Kinetics,* **36**, 2004, 603-622.

[2] Li, J., Zhao, Z., Kazakov, A., Chaos, M., Dryer, F.L., and Scire Jr., J.J., *International Journal of Chemical Kinetics*, **39**, 2007, 109-136.

[3] Davis, S.G., Joshi, A.V., Wang, H., *Proc. Combust. Inst.*, **30**, 2005, 1283-1292.

[4] Smith, G.P., Golden, D.M., Frenklach, M., Moriarty, N.W., Eiteneer, B., Goldenberg, M., Bowman, C.T., Hanson, R.K., Song, S., Gardiner, W.C., Lissianski, V.V., Qin, Z. http://www.me.berkeley.edu/gri_mech.

[5] Joshi, A.V., Wang, H., *Int. J. Chem. Kinet.,* **38**, 2006, 57-73.

[6] Sivaramakrishnan, R., Comandini, A., Tranter, R.S., Brezinsky, K., Davis, S.G., Wang, H., *Proc. Combust. Inst.*, **31**, 2007, 429-437.

[7] Hochanadel, C. J., Sworski, T. J. and Ogren, P. J., *J. Phys. Chem.,* **84**, 1980, 3274-3277.

[8] Lii, R. R., Gorse, R. A., Sauer, M. C. and Gordon, S., *J. Phys. Chem.,* **84**, 1980, 819-821.

[9] Cox, R. A., Burrows, J. P. and Wallington, T. J., *Chem. Phys. Lett.,* **84**, 1981, 217-221.

[10] Kaufman, F., *J. Photochem.,* **17**, 1981, 397-404.

[11] Thrush, B. A. and Wilkinson, J. P. T., *Chem. Phys. Lett.,* **81**, 1981, 1-3.

[12] Rozenshtein, V. B., Gershenzon, Y. M., Ilin, S. D. and Kishkovitch, O. P., *Chem. Phys. Lett.,* **112**, 1984, 473-478.

[13] Sridharan, U. C., Qiu, L. X. and Kaufman, F., *J. Phys. Chem.,* **88**, 1984, 1281-1282.

[14] Temps, F. and Wagner, H. G., *Ber. Bunsenges. Phys. Chem.,* **88**, 1984, 415-418.

[15] Dransfeld, P. and Wagner, H. G., *Z. Naturforsch.,* **42a**, 1987, 471-476.

[16] Keyser, L. F., *J. Phys. Chem.,* **92**, 1988, 1193-1200.

[17] Schwab, J. J., Brune, W. H. and Anderson, J. G., *J. Phys. Chem.,* **93**, 1989, 1030-1035.

[18] Kijewski, H. and Troe, J., *Int. J. Chem. Kinet.,* **3**, 1971, 223-235.

[19] Hippler, H. and Troe, J., *Chem. Phys. Lett.,* **192**, 1992, 333-337.

[20] Hippler, H., Neunaber, H. and Troe, J., *J. Chem. Phys.,* **103**, 1995, 3510-3516.

[21] Kappel, C., Luther, K. and Troe, J., *Phys. Chem. Chem. Phys.,* **4**, 2002, 4392-4398.

[22] Sivaramakrishnan, R., Comandini, A., Tranter, R.S., Brezinsky, K., Davis, S.G. and Wang, H., *Proc.Combust. Inst.,* **31**, 2007, 429-437.

[23] Srinivasan, N.K., Su, M.C., Sutherland, J.W., Michael, J.V. and Ruscic, B., *J. Phys. Chem.,* **110**, 2006, 6602-6607.

[24] Goodings, J. M. and Hayhurst, A. N., *J. Chem. Soc. Faraday Trans. II,* **84**, 1988, 745-762.

[25] Gonzalez, C., Theisen, J., Schlegel, H. B., Hase, W. L. and Kaiser, E. W., *J. Phys. Chem.,* **96**, 1992, 1767-1774.

6. BIBLIOGRAPHY

1. G. Mittal, C.J. Sung, M. Fairweather, A.S. Tomlin, J.F. Griffiths, and K.J. Hughes, "Significance of the HO_2+CO Reaction during the Combustion of CO+H_2 Mixtures at High Pressures," *Proceedings of the Combustion Institute*, Vol. 31, 419-427, 2007.
2. R. Sivaramakrishnan, A. Comandini, R.S. Tranter, K. Brezinsky, S.G. Davis, and H. Wang, "Combustion of CO/H_2 Mixture at Elevated Pressures," *Proceedings of the Combustion Institute*, Vol. 31, 429-437, 2007.
3. X. You, E. Goos, C.J. Sung, and H. Wang, "Reaction Kinetics of CO+HO_2→CO_2+OH ab initio Study and Master Equation Modeling," work-in-progress poster, 31st International Symposium on Combustion, Heidelberg, Germany, August 2006.
4. G. Mittal and C.J. Sung "Ignition of Moist Syngas in a Rapid Compression Machine", 5th US Combustion Meeting, San Diego, March 2007.
5. X. You, H. Wang, E. Goos, C.J. Sung, and S. J. Klippenstein "Reaction Kinetics of CO+HO_2 → Products: ab initio Study and Master Equation Modeling," 5th US Combustion Meeting, San Diego, March 2007.
6. X. You, H. Wang, E. Goos, C.J. Sung, and S. J. Klippenstein "Reaction Kinetics of CO+HO_2 → Products: ab initio Study and Master Equation Modeling," *Journal of Physical Chemistry A*, Vol. 111, 4031-4042, 2007.
7. C.J. Sung and C.K. Law "Fundamental Combustion Properties of H_2/CO Mixtures: Ignition and Flame Propagation at Elevated Pressures," *Combustion Science and Technology* 180 (6), 1097-1116, 2008.
8. A.K. Das, K. Kumar, and C.J. Sung "Laminar Flame Speeds of moist H_2/CO mixtures", Proceedings of the 2008 Technical Meeting of the Central States Section of the Combustion Institute, Tuscaloosa, April 2008.
9. A.K. Das, C.J. Sung, and G. Mittal, "Ignition Delay Study of Moist Syngas Mixtures Using a Rapid Compression Machine", 6th US Combustion Meeting, Ann Arbor, May 2009.
10. A.K. Das, K. Kumar, and C.J. Sung "Laminar Flame Speeds of Moist Syngas Mixtures", 6th US Combustion Meeting, Ann Arbor, May 2009.